How to cite: *Angew. Chem. Int. Ed.* **2021**, *60*, 18876–18881
International Edition: doi.org/10.1002/anie.202104469
German Edition: doi.org/10.1002/ange.202104469

Photoelectrocatalysis

Thiophene-Based Conjugated Acetylenic Polymers with Dual Active Sites for Efficient Co-Catalyst-Free Photoelectrochemical Water Reduction in Alkaline Medium

Mino Borrelli[+], Christine Joy Querebillo[+], Dominik L. Pastoetter, Tao Wang, Alberto Milani, Carlo Casari, Hoang Khoa Ly, Fan He, Yang Hou, Christof Neumann, Andrey Turchanin, Hanjun Sun, Inez M. Weidinger,* and Xinliang Feng**

Abstract: *Although being attractive materials for photoelectrochemical hydrogen evolution reaction (PEC HER) under neutral or acidic conditions, conjugated polymers still show poor PEC HER performance in alkaline medium due to the lack of water dissociation sites. Herein, we demonstrate that tailoring the polymer skeleton from poly(diethynylthieno[3,2-b]thiophene) (**pDET**) to poly(2,6-diethynylbenzo[1,2-b:4,5-b′]dithiophene (**pBDT**) and poly(diethynyldithieno[3,2-b:2′,3′-d]thiophene) (**pDTT**) in conjugated acetylenic polymers (CAPs) introduces highly efficient active sites for water dissociation. As a result, **pDTT** and **pBDT**, grown on Cu substrate, demonstrate benchmark photocurrent densities of 170 $\mu A\,cm^{-2}$ and 120 $\mu A\,cm^{-2}$ (at 0.3 V vs. RHE; pH 13), which are 4.2 and 3 times higher than that of **pDET**, respectively. Moreover, by combining DFT calculations and electrochemical operando resonance Raman spectroscopy, we propose that the electron-enriched C_β of the outer thiophene rings of **pDTT** are the water dissociation active sites, while the $-C{\equiv}C-$ bonds function as the active sites for hydrogen evolution.*

Introduction

Hydrogen, the "fuel of the future"[1] with its very high energy density (120 $MJ\,kg^{-1}$),[2] is envisioned as a valid solution to the present energy crisis following the exhaustion of fossil fuels and their negative impact on climate. Photoelectrochemical (PEC) water splitting[3] is a promising technology for hydrogen production exploiting the inexhaustible solar energy and the electrolysis of water. So far, PEC HER photocathode materials, such as the visible-light responsive inorganic metal oxides,[4–8] transition-metal dichalcogenides,[9,10] and metal sulphides,[11,12] have been hampered for practical and widespread implementation due to their need of co-catalyst (e.g. Pt) with high costs, increased photocorrosion,[13] and challenges to modulate their electronic properties.

[*] M. Borrelli,[+] D. L. Pastoetter, Prof. H. Sun, Prof. X. Feng
Center for Advancing Electronics Dresden (cfaed) and Department of Chemistry and Food Chemistry
Dresden University of Technology
Mommsenstrasse 4, 01062 Dresden (Germany)
E-mail: hanjun.sun@njnu.edu.cn
xinliang.feng@tu-dresden.de

Dr. C. J. Querebillo,[+] Dr. H. Khoa Ly, Prof. I. M. Weidinger
Chair of Electrochemistry
Department of Chemistry and Food Chemistry
Dresden University of Technology
Zellescher 19, 01062 Dresden (Germany)
E-mail: inez.weidinger@tu-dresden.de

Dr. C. J. Querebillo[+]
Institute for Complex Materials
Leibniz-Institute for Solid State and Materials Research (IFW)
Helmholtzstrasse, 20, 01069 Dresden (Germany)

Prof. T. Wang
Center of Artificial Photosynthesis for Solar Fuels
School of Science, Westlake University
18 Shilongshan Road, Hangzhou 310024, Zhejiang Province (China)

Dr. A. Milani, Prof. C. Casari
Diparimento di Energia, Politecnico di Milano
Via Ponzio 34/3, Milano (Italy)

F. He, Prof. Y. Hou
Key Laboratory of Biological Engineering of Ministry of Education
College of Chemical and Biological Engineering
Zhejiang University
Hangzhou 310027 (China)

Dr. C. Neumann, Prof. A. Turchanin
Institute of Physical Chemistry and Center for Energy and Environmental Chemistry Jena (CEEC Jena)
Friedrich Schiller University Jena
Lessingstrasse 10, 07743 Jena (Germany)

Prof. H. Sun
Jiangsu Key Laboratory of New Power Batteries
Jiangsu Collaborative Innovation Centre of Biomedical Functional Materials
School of Chemistry and Materials Science
Nanjing Normal University
1 Wenyuan Road, Nanjing 210023 (China)

[+] These authors contributed equally to this work.

Supporting information and the ORCID identification number(s) for the author(s) of this article can be found under: https://doi.org/10.1002/anie.202104469.

Recently, synthetic organic materials,[14–16] such as polythiophenes,[17–19] graphitic carbon nitrides,[20,21] and conjugated acetylenic polymers,[22–24] have emerged as an exciting class of photocathode materials due to their fascinating peculiarities. The delocalized electron system, the broader absorption of the solar spectrum (narrower band gap), molecular-level tunability of band gap and energy level positions, facile synthesis, and low-cost processing are amongst the main advantages. As yet, most of the reported synthetic organic material-based photocathodes for PEC HER have been carried out at neutral or acidic conditions (facilitated by high concentration of protons), while only a few examples[17,19] have been demonstrated in alkaline medium. The HER at high pH requires an additional energy barrier to overcome for splitting water (water dissociation step)[25] and producing protons, resulting in a typically 2–3-fold lower catalytic activity than in acidic medium even with Pt as co-catalyst.[26] The development of efficient and stable photocathodes working at high pH is envisioned as a possible pathway to increase the overall PEC water splitting efficiency,[27] currently undermined by the sluggish kinetics and consequently high overpotential of the photoanodes where the oxygen evolution reaction (OER) occurs. Such photocathodes could be coupled with highly active and stable OER catalysts or solar cells, whose stability is higher in the alkaline medium,[17] or with photoanodes in the unassisted solar water splitting.[28] However, at present, it is still a significant challenge to develop conjugated polymers with active sites for both water dissociation and hydrogen evolution.

Driven by the above considerations, we developed thiophene-based conjugated acetylenic polymers (CAPs) for HER in alkaline medium with highly efficient dual active sites for both water dissociation and hydrogen evolution. By modifying the thiophene skeleton from poly(2,5-diethynylthieno[3,2-*b*]thiophene) (**pDET**) to poly(2,6-diethynylbenzo[1,2-*b*:4,5-*b*′]dithiophene (**pBDT**) and poly(2,6-diethynyldithieno[3,2-*b*:2′,3′-*d*]thiophene) (**pDTT**), which are grown on Cu foam substrates, highly efficient water dissociation sites are incorporated in the polymer structures (Figure 1b). Among those, pDTT/Cu presents an impressive photocurrent density of approximately 170 μA cm^{-2} at 0.3 V vs. reversible hydrogen electrode (RHE) in 0.1 M KOH (pH 13) under AM1.5G irradiation, which is 4.2 times higher than poly(2,5-diethynylthieno[3,2-*b*]thiophene), **pDET**/Cu. The performance of **pDTT**/Cu thus exceeds those of reported co-catalyst-free polythiophenes[17,19] and even co-catalyst-free inorganic materials in acidic/neutral medium.[9,10,29] By combining investigations from electrochemical operando Raman Spectroscopy[30,31] and density functional theory (DFT), we propose that the water dissociation process occurs via a charge density transfer from the middle ring of the dithieno[3,2-*b*:2′,3′-*d*]thiophene moieties of **pDTT** towards the outer thiophene rings and the diacetylenic linkages. The water reduction occurs with the single-site Volmer–Heyrovsky pathway with the as-produced proton bonded to the −C≡C− atom (closest to the thiophene skeleton). This work represents a new understanding of the photoelectrocatalytic water reduction in organic materials and leads the way to develop new materials with improved performance.

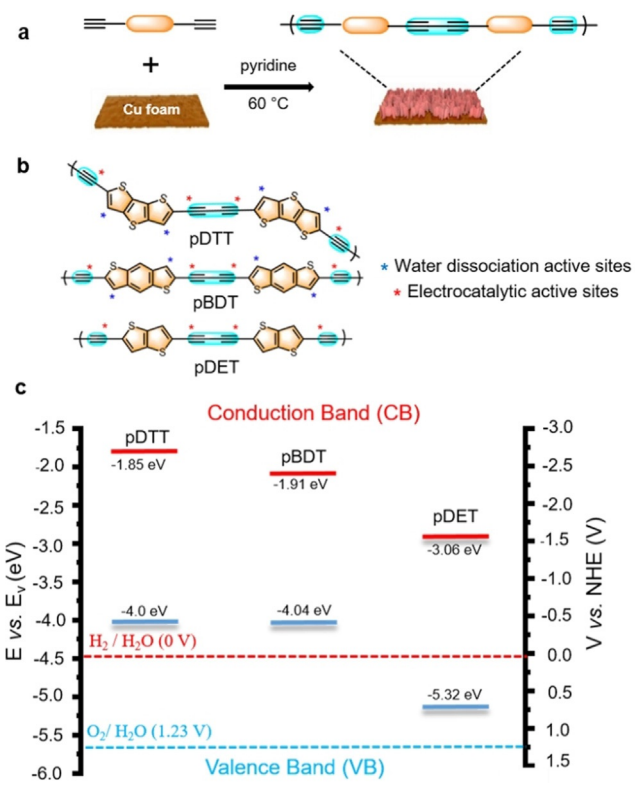

Figure 1. Synthesis and characterization of conjugated acetylenic polymers (CAPs) on commercial Cu foam. a) Synthesis of CAPs using a copper-mediated Glaser polycondensation method on the Cu foam. b) Chemical structures of the polymers **pDTT**, **pBDT** and **pDET**. c) Optical and electronic properties of **pDTT**, **pBDT**, and **pDET**. Diagram of band positions of the polymers with the H_2O/H_2 (HER) and O_2/H_2O (OER) redox couples.

Results and Discussion

Materials Synthesis and Characterization: The polymers were synthesized on commercial Cu foam (1 × 3 cm^2, CAPs/Cu) as displayed in Figure 1a. As previously reported,[22,32] a copper source (foil or foam) in contact with a polar solvent releases Cu^I and Cu^{II} ions that catalyze the in situ C–C Glaser oxidative coupling. The Cu foam works as both catalyst and conductive substrate providing excellent ohmic contact with the overlying polymer. **pDTT** and **pBDT** were successfully synthesized within 6 h in a pyridine solution containing the monomer (0.25 mg mL^{-1}) and piperidine (16 μL). A dense vertically aligned and interconnected nanosheet layer was observed via scanning electron microscopy (Figure S4a,b). Focused ion beam was employed to measure the cross section of **pDTT**/Cu (Figure S4c,d), revealing an average thickness of 160–190 nm. **pDET** and **pBDT** showed a similar sheet-like morphology (Figure S5). The chemical compositions of **pDTT**, **pDET**, and **pBDT** were analyzed through resonance Raman (RR) spectroscopy and X-ray photoelectron spectroscopy (XPS). RR confirmed the successful polymerization on Cu foam as depicted in Figure S6 and Figure 4a. Based on DFT calculations (Figure S11), characteristic peaks for the CAPs/Cu are assigned: C–S stretches (1100–1250 cm^{-1}), C–C ring stretches (1200–1600 cm^{-1} for C_α–C_β; 1350–1500 cm^{-1}

for C_β–C_β), ring deformations (1100–1500 cm^{-1}), ring expansion/contraction (1300–1450 cm^{-1}), and −C≡C− bonds (1900–2200 cm^{-1}, with 1920–1935 cm^{-1} for the −C≡C−/Cu interaction). The deconvolution of high-resolution C1s core level XPS reports the sp-carbon signal of **pDTT** and **pBDT** (Figure S7 and S8) at 284.2 and 284.0 eV, respectively; **pDET** is depicted at a slightly lower energy (283.6 eV).[23] Both XPS and RR are related to the electron density and the chemical environment. The following trend for the −C≡C− bond energy was identified: **pDET** < **pBDT** < **pDTT**, suggesting that the increase in the conjugation (donor character) of the thiophene skeleton pushes less electron density into the diacetylenic linkages, thus strengthening the −C≡C− bonds.

Ultraviolet-visible absorption spectroscopy (UV/Vis) and ultraviolet photoelectron spectroscopy (UPS) spectra were measured to determine the optical band gaps and energy levels, respectively. As illustrated in Figure S9, **pDTT** and **pBDT** have a similar absorption edge at ca. 510 nm, resulting in comparable band gaps (2.25 and 2.23 eV). The absorption edge of **pDET**, instead, is shifted to 500 nm[23] with a band gap of 2.26 eV. Valence band (VB) positions of **pDTT** and **pBDT** were determined via UPS at ca. −4 eV (Figure S10), while VB of **pDET** is at −5.32 eV.[23] Based on the formula $E_{CB} = E_{VB} +$ optical band gap (eV), the conduction band levels (E_{CB}) were calculated to be −1.85 eV and −1.91 eV for **pDTT** and **pBDT**. Compared to the standard HER potential (0 V vs. NHE), the CAPs showed more negative E_{CB}, thus satisfying the thermodynamic requirements for the water reduction (Figure 1c).

Photoelectrochemical Tests: As depicted in the linear sweep voltammetry (LSV) under solar light illumination (AM1.5G, 100 mW cm^{-2}) in Figure S12, the bare Cu foam did not show any response, underlining that the PEC performance originated from the polymers grown on the Cu foam. Figure 2a shows typical on/off switching behavior of the polymers. From the same graph, it appears evident that all the CAPs/Cu present a clear reduction peak. Such feature is due to the electrochemical reduction of Cu^+ to Cu as observed in the bare Cu foam (Figure S13–S15) without light irradiation.

A typical capacitive behavior of conjugated polymers under applied bias is also expected to contribute to the overall dark current.[33] *J*–*t* curves at high potentials were also employed to find the onset potentials of the CAPs. Remarkably, all the CAPs had onset potentials as low as 1 V vs. RHE (Figure S16). Under solar illumination, **pDTT**/Cu provided a photocurrent density of approximately 140 and 170 μA cm^{-2} at 0 V and 0.3 V vs. RHE, respectively (Figure S17). **pBDT**/Cu, instead, reached a value of approximately 100 and 120 μA cm^{-2} at 0 V and 0.3 V vs. RHE, respectively (Figure 2b). The photocurrent generated from **pDTT**/Cu thus exceeds previously reported co-catalyst-free polythiophenes, polyterthiophene (pTTh)[19] and poly(1,4-di(2-thienyl))benzene (pDTB)[17] (120 and 128 μA cm^{-2} at pH 11, respectively), co-catalyst-free organic photocathodes in neutral medium, such as g-C_3N_4 (1–45 μA cm^{-2} at pH 6.8/7),[21,34] covalent organic frameworks (COFs),[35–37] as well as co-catalyst-free chalcopytire $CuInS_2$ (ca. 30 μA cm^{-2} at pH 5),[11] inorganic oxides NiO (ca. 30 μA cm^{-2} at pH 1),[29] and even transition-metal dichalcogenides, WSe_2 (ca. 40 μA cm^{-2} at pH 0)[9] (Figure 2d and Table S1). Meanwhile, pDET/Cu as the reported state-of-the-art of co-catalyst-free organic photocathodes[23] with an outstanding photocurrent density of approximately 370 μA cm^{-2} at 0.3 V vs. RHE in neutral medium (0.1 M Na_2SO_4, pH 6.8) only reached a photocurrent density of approximately 40 μA cm^{-2} at 0.3 V vs. RHE at pH 13. Although **pDET** possessed the lowest conduction band, which is more favorable thermodynamically, the lower performance implied that **pDET** lacked the active sites for water dissociation, as presented in both **pDTT** and **pBDT**. Due to the relatively high dark current, we could not measure the charge separation efficiency or the photocurrent density values at the different wavelengths to obtain the IPCE (incident photon-to-electron conversion efficiency) spectrum of the CAPs at pH 13. A more powerful or an additional light source[38] will be needed in future work.

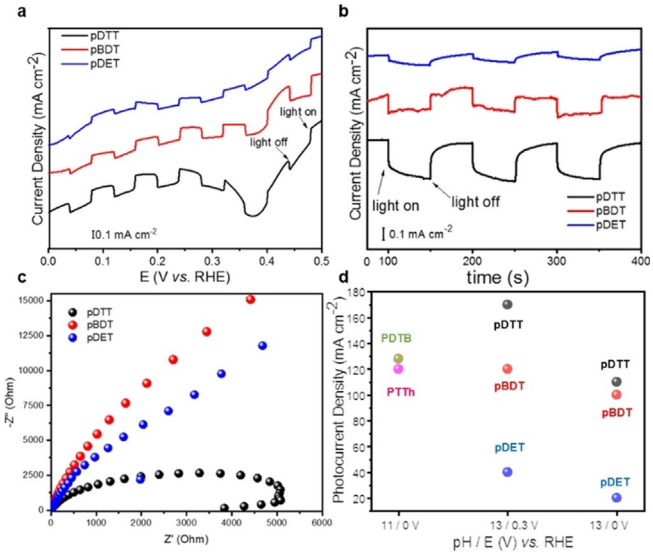

Figure 2. Photoelectrochemical HER performance in 0.1 M KOH (pH 13). a) Linear Sweep Voltammetry of the CAPs recorded at 2 mV s^{-1}. b) Amperometric responses of the CAPs at 0.3 V vs. RHE c) Electrochemical impedance spectroscopy (EIS) at 0 V vs. RHE collected without light irradiation. d) Performance of the polymers employed here in comparison with the state of the art.

The long-term PEC HER at 0.3 V vs. RHE was also measured. After 10 h of continuous measurement under solar light illumination at pH 13, **pDTT** could retain more than 75% of the initial photocurrent density value (Figure S18). Raman spectroscopy demonstrated only minor changes in the main peaks of **pDTT** before and after 10 h of continuous operation (Figure S19). Furthermore, the evolved gaseous product generated from **pDTT** was analyzed using a gas chromatograph (GC) coupled with a TCD detector. The experimentally measured Faraday efficiency (FE) in phosphate buffer (pH 9) reached almost 90%. However, due to the large dark current and the lower stability, the exact FE value at pH 13 was difficult to obtain.

Charge Transfer: To gain more insights into the superior performance of **pDTT** in the alkaline electrolyte, electrochemical impedance spectroscopy (EIS) was employed to analyze the charge transfer resistance (R_{CT}) of the polymers. In Figure 2c, Nyquist plots of the polymers without light

irradiation are shown. The fitted values for the semi-circles are (2360 ± 15) Ω for **pDTT**, (10000 ± 25) Ω for **pBDT**, and (6740 ± 20) Ω for **pDET**, revealing the following R_{CT} trend: **pBDT** > **pDET** > **pDTT**. When irradiated (Figure S20) the R_{CT} drastically went down to (8850 ± 25) Ω for **pBDT**, and (4035 ± 20) Ω for **pDET**. A less significant reduction for **pDTT** (1980 ± 20) Ω was measured. The EIS results clearly indicated that the dithieno[3,2-*b*:2′,3′-*d*]thiophene structures of **pDTT** benefitted the charge transfer process on the photocathode, while the benzo[1,2-*b*:4,5-*b*′]dithiophenes in **pBDT** were found to be the most detrimental for the R_{CT} (Figure S20).

Understanding the Active Sites: To reveal the catalytic active sites of the CAPs for PEC HER, DFT simulations of their hydrogen binding free energies[39,40] were performed. As clearly visible in Figure 3a, in the alkaline medium (pH 13), **pDTT** revealed the lowest free energy (0.32 eV), resulting in

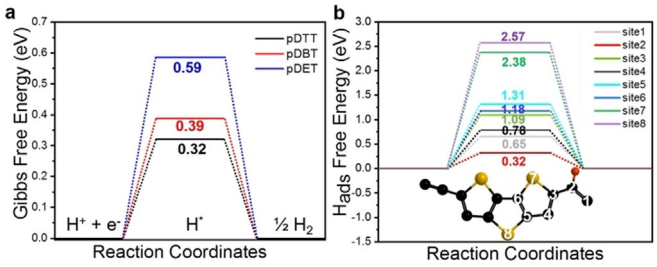

Figure 3. DFT simulations to investigate active sites and H_2 evolution reaction activities on different polymers. a) Free-energy diagrams for HER on **pDTT**, **pBDT**, and **pDET** polymers at 0 V vs. RHE and pH 13. b) Free-energy diagram for H_2 evolution via Volmer–Heyrovsky reaction route at 0 V vs. RHE: 1, 2, 3, 4, 5, 6, 7, 8 denote different active sites of **pDTT** (black sphere for carbon, yellow for sulfur, red for the bonded proton). Hydrogen atoms of the polymer have been omitted for clarity.

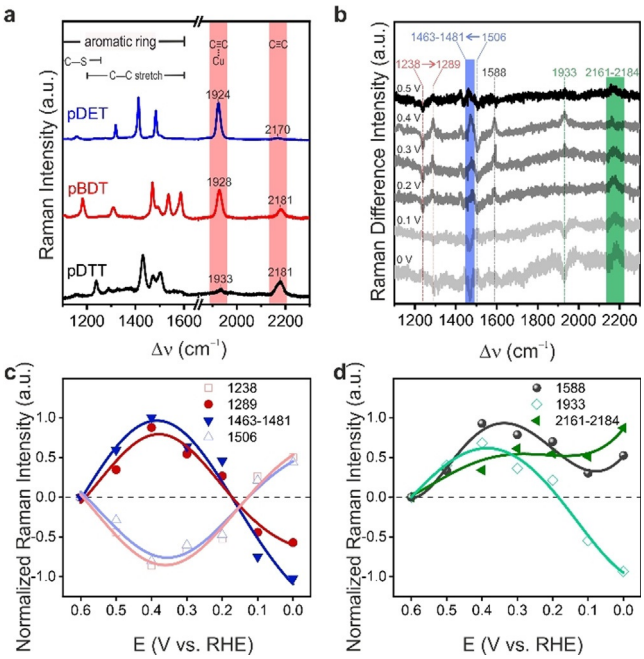

Figure 4. Operando resonance Raman spectra of CAPs/Cu in 0.1 M KOH. Spectra were obtained under 561 nm laser. a) Resonance Raman spectra of CAPs/Cu at open circuit (OCP). Red highlights indicate bands related to −C≡C− bonds. b) Potential-dependent difference Raman spectra of **pDTT**/Cu. The difference spectra at each potential are against the spectrum taken at 0.6 V. c) Potential-dependent difference intensities of the Raman bands at 1238, 1289, 1463–1481, and 1506 cm^{-1} for **pDTT**/Cu. d) Potential-dependent difference intensities of the Raman bands at 1588, 1933, and 2161–2184 cm^{-1} for **pDTT**/Cu.

the most suitable hydrogen binding strength, while **pBDT** and **pDET** displayed values of 0.39 and 0.59 eV, respectively. The calculated trend fits the experimental photocurrent values collected at 0 V vs. RHE. (Figure S21 and S22). Moreover, the Volmer–Tafel reaction pathway was not feasible due to the high energy requirements. Thorough inspections of the Volmer–Heyrovsky mechanism indicated that the C atom in the −C≡C− bonds (site 2) of **pDTT** had the lowest ΔG^{H}_{ads} value (0.32 eV), thus acting as a highly active electrocatalytic center (Figure 3b).

Next, electrochemical operando resonance Raman was employed to give mechanistic insights and to identify possible catalytic intermediates. The potential-dependent difference spectra of **pDTT**/Cu (vs. 0.6 V), as indicated in Figure 4b, showed an apparent upshift of the peak from 1238 to 1289 cm^{-1} and a downshift from 1506 to 1463–1481 cm^{-1} (highlighted in red and blue, respectively). From the DFT calculations (Figure S11 and Supporting Gifs 1 and 2), the 1262 cm^{-1} and the 1519 cm^{-1} shifts were assigned to mainly C_α–C_β stretching modes of the inner and outer thiophene rings, respectively. As the 1506 cm^{-1} peak is shifted to lower wavenumbers and the 1238 cm^{-1} peak to higher wavenumbers, we conclude that a charge density transfer takes place from the middle thiophene ring to the outer ones in the dithieno[3,2-*b*:2′,3′-*d*]thiophene components of **pDTT**. In the difference spectra of **pDET**/Cu (vs. 0.6 V, Figure S23), none of the shifts observed in **pDTT** were detected, therefore confirming the absence of a potential-induced charge transfer in the thieno[3,2-*b*]thiophene units of **pDET**, which is a prerequisite for creating an active site for water dissociation.

Furthermore, the downshifting 1506–1463 cm^{-1} peak gradually shifted up to 1481 cm^{-1} when the potential increased up to 0.2 V, restoring its initial position at 0.1 V and 0 V (Figure S24). In the potential-dependent difference intensity plot (Figure 4c) an absolute maximum difference is clearly visible at 0.4–0.3 V, which fits to the higher photocurrent collected at 0.3 V for **pDTT** (under solar light illumination). Changes in the diacetylenic peaks were also observed (green highlights) with alternating increase in the intensities of the −C≡C−/Cu (1933 cm^{-1}) and −C≡C− (2181 cm^{-1}) vibrations, mainly in the potential region of 0.4–0.2 V (Figure 4d). Orientation effects on this peak cannot be excluded.[41] Noteworthy, the 2181 cm^{-1} peak downshifted by approximately 20 cm^{-1} (2161 cm^{-1} at 0.4 V, Figure S24b). This drastically lowered the energy required to break the −C≡C− bond reaching an even lower value than **pDET**/Cu (2170 cm^{-1}), thus explaining the highest HER of **pDTT**/Cu amongst the CAPs in alkaline medium.

Lastly, we detected the rising of a vibrational band at 1588 cm^{-1}. This peak appeared at 0.6 V but was almost absent (with negligible intensity) in **pDTT** under dry (without electrolyte) and open-circuit (OCP) conditions (Figure S25). A clear assignment of this peak is not possible at the moment. It might correspond to the −C=C− intermediate[31] or be a result from dithienothiophene–water interaction. Additional peaks (1977 and 2095 cm^{-1}) appeared in the triple bond region and were assigned to an intermediate state or transient −C≡C− as observed before.[23]

Proposed Mechanism: To further understand how the hydrogen evolution occurs on **pDTT**/Cu, low-frequency resonance Raman measurements were performed at 561 nm and 594 nm laser excitation. Notably, the slightly lower energy excitation also causes a photo-induced charge separation for the lower-energy vibrational modes (Figure S26). Using the 561 nm excitation, some of the vibrations were shifted to lower wavenumbers in comparison to 594 nm: the 814 cm^{-1} (vs. 819 cm^{-1}) peak, corresponding to the asymmetric C–S stretching of the outer thiophene rings coupled with the symmetric C–S stretching of the inner thiophene ring and the 933 cm^{-1} (vs. 937 cm^{-1}) peak due to the C_α–C_β(H)–C_β scissoring motion that brings the C_β(H) close to the −C≡C− coupled with the diacetylene bending vibrations. These shifts indicate that photoinduced processes mainly take place at the dithienothiophene cores of **pDTT**. As both the 814/819 cm^{-1} and 933/937 cm^{-1} normal modes bring the C_β closer to the diacetylenic moieties, we propose that the water dissociation step occurs via a six-atom intermediate where water interacts with the sufficiently electron rich C_β(H) of the outer thiophene ring. Such C–H(thiophene)···O(water) interaction (Figure S27a) was previously reported[42] to have the most preferred geometry between thiophene and water and it is here proposed to be strong enough to break the (H)O–H bond in the water molecule.

However, the normal modes of interest also involve C–S stretches, providing another possible pathway for proton generation. In such case, the interaction of S(outer thiophene)···H–O(water) is possible with the enriched electron density of the outer thiophene of **pDTT** (Figure S27b). Exhaustive DFT calculations with a B3LYP/6-311++G(d,p) level on the proposed intermediates for the dimer-water were calculated to prove which interaction was more favorable. The hydrogen bond C–H(thiophene)···O(water) distance was calculated to be 2.32 Å, while the distance O–H···C(triple bond) was 2.76 Å. These values are within the range of typical hydrogen bond lengths.[43] The other proposed intermediate S(outer thiophene)···H–O(water) geometry was not predicted.

To sum up the aforesaid discussion, we propose that the hydrogen evolution in alkaline medium on **pDTT** occurs with the following steps (Figure 5): a photoinduced charge separation causes the outer thiophenes of **pDTT** to be electron dense (1) becoming active sites for interacting with water. This interaction leads to the water dissociation step (2) providing the proton needed for the Volmer Step (3) to occur on site 2 (Figure 3b). The hydrogen release bringing the catalyst back to its ground state occurs via the Heyrovsky Step (4) (Figure 5).

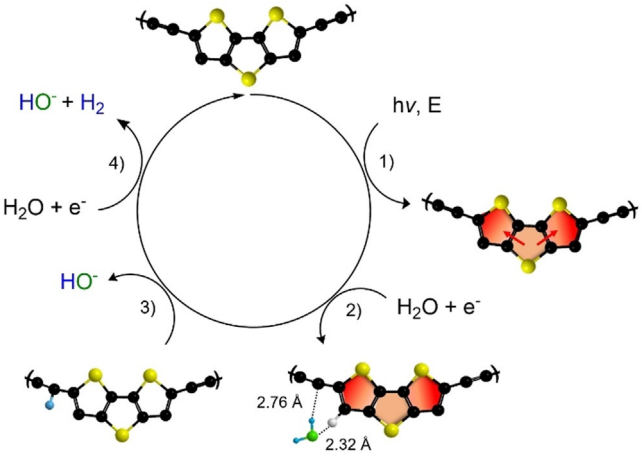

Figure 5. Proposed mechanism of HER in alkaline medium for **pDTT**.

Conclusion

In this work, we demonstrate thiophene-based conjugated acetylenic polymers as highly efficient photocathodes in alkaline medium by introducing dual active sites for the water dissociation and hydrogen evolution. Among them, **pDTT** on commercial Cu foam displays a benchmark PEC HER performance with a photocurrent density of approximately 170 $\mu A\,cm^{-2}$ at 0.3 V vs. RHE under solar light irradiation. By combining findings from DFT and electrochemical operando RR spectroscopy, we propose that the photoactivated C_β of the outer thiophenes of the dithieno[3,2-*b*:2′,3′-*d*]thiophene moieties and the triple bonds cooperate as dual active sites to evolve hydrogen at high pH. This understanding sheds new insight into organic materials not only for water splitting but also for other photoelectrocatalytic processes (N_2 reduction, CO_2 fixation) and most certainly will pave the way for the synthesis of new and more efficient materials.

Acknowledgements

This work was financially supported by the Graphene Flagship (GrapheneCore3, No. 881603) and ERC Grant (T2DCP, No. 819698). We acknowledge the cfaed (Center for Advancing Electronics Dresden) and the Dresden Center for Nanoanalysis (DCN) at TU Dresden. I.W. acknowledges the cluster of excellence UniSysCat (EXC 2008/1-390540038). C.S. and A.M. acknowledge ERC Grant (CoG 2016 EspLORE, No. 724610). A.T. and C.N. acknowledge DFG TRR 234 "CataLight" (B7 and Z2) and research infrastructure grant INST 275/257-1. M.B. thanks Dr. Tao Zhang, Huanhuan Shi, Dr. Markus Löffler (DCN), and Dr. Zhongquan Liao for preliminary characterization, Dr. Moritz Kuehnel and Dr. Uttam Gupta for preliminary measurements, Dr. Jian Zhang and Dr. Ahiud Morag for fruitful discussions, and Prof. Fabrizia Negri for preliminary calculations. C.J.Q. acknowledges Markus Göbel for his helpful suggestions. Open access funding enabled and organized by Projekt DEAL.

Conflict of Interest

The authors declare no conflict of interest.

Keywords: alkaline medium · co-catalyst-free photocathodes · conjugated polymers · dual sites · hydrogen evolution

[1] N. Armaroli, V. Balzani, *ChemSusChem* **2011**, *4*, 21 – 36.
[2] L. Mascaretti, A. Dutta, Š. Kment, V. M. Shalaev, A. Boltasseva, R. Zbořil, A. Naldoni, *Adv. Mater.* **2019**, *31*, 1805513.
[3] M. Grätzel, *Nature* **2001**, *414*, 338 – 344.
[4] A. Landman, H. Dotan, G. E. Shter, M. Wullenkord, A. Houaijia, A. Maljusch, G. S. Grader, A. Rothschild, *Nat. Mater.* **2017**, *16*, 646 – 651.
[5] A. Paracchino, V. Laporte, K. Sivula, M. Grätzel, E. Thimsen, *Nat. Mater.* **2011**, *10*, 456 – 461.
[6] C. G. Morales-Guio, S. D. Tilley, H. Vrubel, M. Grätzel, X. Hu, *Nat. Commun.* **2014**, *5*, 3059.
[7] P. Dai, W. Li, J. Xie, Y. He, J. Thorne, G. McMahon, J. Zhan, D. Wang, *Angew. Chem. Int. Ed.* **2014**, *53*, 13493 – 13497; *Angew. Chem.* **2014**, *126*, 13711 – 13715.
[8] C. Li, T. Hisatomi, O. Watanabe, M. Nakabayashi, N. Shibata, K. Domen, J. J. Delaunay, *Energy Environ. Sci.* **2015**, *8*, 1493 – 1500.
[9] X. Yu, M. S. Prévot, N. Guijarro, K. Sivula, *Nat. Commun.* **2015**, *6*, 7596.
[10] J. R. McKone, A. P. Pieterick, H. B. Gray, N. S. Lewis, *J. Am. Chem. Soc.* **2013**, *135*, 223 – 231.
[11] J. Luo, S. D. Tilley, L. Steier, M. Schreier, M. T. Mayer, H. J. Fan, M. Grätzel, *Nano Lett.* **2015**, *15*, 1395 – 1402.
[12] S. Y. Chae, S. J. Park, S. G. Han, H. Jung, C. W. Kim, C. Jeong, O. S. Joo, B. K. Min, Y. J. Hwang, *J. Am. Chem. Soc.* **2016**, *138*, 15673 – 15681.
[13] S. Chen, D. Huang, P. Xu, W. Xue, L. Lei, M. Cheng, R. Wang, X. Liu, R. Deng, *J. Mater. Chem. A* **2020**, *8*, 2286 – 2322.
[14] S. Otep, T. Michinobu, Q. Zhang, *Sol. RRL* **2020**, *4*, 1900395.
[15] L. Yao, A. Rahmanudin, N. Guijarro, K. Sivula, *Adv. Energy Mater.* **2018**, *8*, 1802585.
[16] G. Zhang, Z.-A. Lan, X. Wang, *Angew. Chem. Int. Ed.* **2016**, *55*, 15712 – 15727; *Angew. Chem.* **2016**, *128*, 15940 – 15956.
[17] K. Oka, K. Noguchi, T. Suga, H. Nishide, B. Winther-Jensen, *Adv. Energy Mater.* **2019**, *9*, 1803286.
[18] C. H. Ng, C. A. Ohlin, S. Qiu, C. Sun, B. Winther-Jensen, *Catal. Sci. Technol.* **2016**, *6*, 3253 – 3262.
[19] K. Oka, O. Tsujimura, T. Suga, H. Nishide, B. Winther-Jensen, *Energy Environ. Sci.* **2018**, *11*, 1335 – 1342.
[20] X. Wang, K. Maeda, A. Thomas, K. Takanabe, G. Xin, J. M. Carlsson, K. Domen, M. Antonietti, *Nat. Mater.* **2009**, *8*, 76 – 80.
[21] Y.-Y. Han, X.-L. Lu, S.-F. Tang, X.-P. Yin, Z.-W. Wei, T.-B. Lu, *Adv. Energy Mater.* **2018**, *8*, 1702992.
[22] T. Zhang, Y. Hou, V. Dzhagan, Z. Liao, G. Chai, M. Löffler, D. Olianas, A. Milani, S. Xu, M. Tommasini, D. R. T. Zahn, Z. Zheng, E. Zschech, R. Jordan, X. Feng, *Nat. Commun.* **2018**, *9*, 1140.
[23] H. Sun, I. H. Öner, T. Wang, T. Zhang, O. Selyshchev, C. Neumann, Y. Fu, Z. Liao, S. Xu, Y. Hou, A. Turchanin, D. R. T. Zahn, E. Zschech, I. M. Weidinger, J. Zhang, X. Feng, *Angew. Chem. Int. Ed.* **2019**, *58*, 10368 – 10374; *Angew. Chem.* **2019**, *131*, 10476 – 10482.
[24] H. Sun, C. Neumann, T. Zhang, M. Löffler, A. Wolf, Y. Hou, A. Turchanin, J. Zhang, X. Feng, *Adv. Mater.* **2019**, *31*, 1900961.
[25] X. Wang, Y. Zheng, W. Sheng, Z. J. Xu, M. Jaroniec, S. Z. Qiao, *Mater. Today* **2020**, *36*, 125 – 138.
[26] N. Mahmood, Y. Yao, J.-W. Zhang, L. Pan, X. Zhang, J.-J. Zou, *Adv. Sci.* **2018**, *5*, 1700464.
[27] C. G. Morales-Guio, L. Liardet, M. T. Mayer, S. D. Tilley, M. Grätzel, X. Hu, *Angew. Chem. Int. Ed.* **2015**, *54*, 664 – 667; *Angew. Chem.* **2015**, *127*, 674 – 677.
[28] S. Ida, K. Yamada, T. Matsunaga, H. Hagiwara, Y. Matsumoto, T. Ishihara, *J. Am. Chem. Soc.* **2010**, *132*, 17343 – 17345.
[29] K. A. Click, D. R. Beauchamp, Z. Huang, W. Chen, Y. Wu, *J. Am. Chem. Soc.* **2016**, *138*, 1174 – 1179.
[30] C. J. Querebillo, I. H. Öner, P. Hildebrandt, K. H. Ly, I. M. Weidinger, *Chem. Eur. J.* **2019**, *25*, 16048 – 16053.
[31] H. K. Ly, I. Weidinger, *Chem. Commun.* **2021**, *57*, 2328 – 2234.
[32] G. Li, Y. Li, H. Liu, Y. Guo, Y. Li, D. Zhu, *Chem. Commun.* **2010**, *46*, 3256 – 3258.
[33] X. Lu, Z. Liu, J. Li, J. Zhang, Z. Guo, *Appl. Catal. B* **2017**, *209*, 657 – 662.
[34] Y. Zhang, T. Mori, J. Ye, M. Antonietti, *J. Am. Chem. Soc.* **2010**, *132*, 6294 – 6295.
[35] S. Xu, H. Sun, M. Addicoat, B. P. Biswal, F. He, S. Park, S. Paasch, T. Zhang, W. Sheng, E. Brunner, Y. Hou, M. Richter, X. Feng, *Adv. Mater.* **2021**, *33*, 2006274.
[36] T. Sick, A. G. Hufnagel, J. Kampmann, I. Kondofersky, M. Calik, J. M. Rotter, A. Evans, M. Döblinger, S. Herbert, K. Peters, D. Böhm, P. Knochel, D. D. Medina, D. Fattakhova-Rohlfing, T. Bein, *J. Am. Chem. Soc.* **2018**, *140*, 2085 – 2092.
[37] D. L. Pastoetter, S. Xu, M. Borrelli, M. Addicoat, B. P. Biswal, S. Paasch, A. Dianat, H. Thomas, R. Berger, S. Reineke, E. Brunner, G. Cuniberti, M. Richter, X. Feng, *Angew. Chem. Int. Ed.* **2020**, *59*, 23620 – 23625; *Angew. Chem.* **2020**, *132*, 23827 – 23832.
[38] P. Bornoz, M. S. Prévot, X. Yu, N. Guijarro, K. Sivula, *J. Am. Chem. Soc.* **2015**, *137*, 15338 – 15341.
[39] B. Hinnemann, P. G. Moses, J. Bonde, K. P. Jørgensen, J. H. Nielsen, S. Horch, I. Chorkendorff, J. K. Nørskov, *J. Am. Chem. Soc.* **2005**, *127*, 5308 – 5309.
[40] W. Sheng, Z. Zhuang, M. Gao, J. Zheng, J. G. Chen, Y. Yan, *Nat. Commun.* **2015**, *6*, 5848.
[41] R. Götz, K. H. Ly, P. Wrzolek, A. Dianat, A. Croy, G. Cuniberti, P. Hildebrandt, M. Schwalbe, I. M. Weidinger, *Inorg. Chem.* **2019**, *58*, 10637 – 10647.
[42] J. G. Wasserman, K. J. Murphy, J. J. Newby, *J. Phys. Chem. A* **2019**, *123*, 10406 – 10417.
[43] T. K. Harris, A. S. Mildvan, *Proteins Struct. Funct. Genet.* **1999**, *35*, 275 – 282.

Manuscript received: March 31, 2021
Revised manuscript received: June 22, 2021
Accepted manuscript online: June 25, 2021
Version of record online: July 14, 2021

